

The role of initial signals in the tropical Pacific Ocean in predictions of negative Indian Ocean Dipole events

FENG Rong and DUAN Wansuo

Citation: [SCIENCE CHINA Earth Sciences](#) ; doi: 10.1007/s11430-018-9296-2

View online: <http://engine.scichina.com/doi/10.1007/s11430-018-9296-2>

Published by the [Science China Press](#)

Articles you may be interested in

[Two modes of dipole events in tropical Indian Ocean](#)

Science in China Series D-Earth Sciences **52**, 369 (2009);

[North Indian Ocean tropical cyclone activities influenced by the Indian Ocean Dipole mode](#)

SCIENCE CHINA Earth Sciences **56**, 855 (2013);

[IOD-related optimal initial errors and optimal precursors for IOD predictions from reanalysis data](#)

SCIENCE CHINA Earth Sciences **60**, 156 (2017);

[The tropical Pacific-Indian Ocean temperature anomaly mode and its effect](#)

Chinese Science Bulletin **51**, 2878 (2006);

[Indian Ocean temperature dipole and SSTA in the equatorial Pacific Ocean](#)

Chinese Science Bulletin **47**, 236 (2002);

The role of initial signals in the tropical Pacific Ocean in predictions of negative Indian Ocean Dipole events

Rong FENG¹ & Wansuo DUAN^{1,2*}

¹ *LASG, Institute of Atmospheric Physics, Chinese Academy of Sciences, Beijing 100029, China;*

² *University of Chinese Academy of Sciences, Beijing 100049, China*

Received August 23, 2018; revised September 26, 2018; accepted November 15, 2018

Abstract Using reanalysis data, the role of initial signals in the tropical Pacific Ocean in predictions of negative Indian Ocean Dipole (IOD) events were analyzed. It was found that the summer predictability barrier (SPB) phenomenon exists in predictions, which is closely related to initial sea temperature errors in the tropical Pacific Ocean, with type-1 initial errors presenting a significant west-east dipole pattern in the tropical Pacific Ocean, and type-2 initial errors showing the opposite spatial pattern. In contrast, SPB-related initial sea temperature errors in the tropical Indian Ocean are relatively small. The initial errors in the tropical Pacific Ocean induce anomalous winds in the tropical Indian Ocean by modulating the Walker circulation in the tropical oceans. In the first half of the prediction year, the anomalous winds, combined with the climatological winds in the tropical Indian Ocean, induce a basin-wide mode of sea surface temperature (SST) errors in the tropical Indian Ocean. With the reversal of the climatological wind in the second half of the prediction year, a west-east dipole pattern of SST errors appears in the tropical Indian Ocean, which is further strengthened under the Bjerknes feedback, yielding a significant SPB. Moreover, two types of precursors were also identified: a significant west-east dipole pattern in the tropical Pacific Ocean and relatively small temperature anomalies in the tropical Indian Ocean. Under the combined effects of temperature anomalies in the tropical Indian and Pacific oceans, northwest wind anomalies appear in the tropical Indian Ocean, which induce a significant west-east dipole pattern of SST anomalies, and yield a negative IOD event.

Keywords Negative Indian Ocean Dipole, Precursor, Initial errors, Pacific Ocean

Citation: Feng R, Duan W. 2018. The role of initial signals in the tropical Pacific Ocean in predictions of negative Indian Ocean Dipole events. *Science China Earth Sciences*, 61, <https://doi.org/10.1007/s11430-018-9296-2>

1. Introduction

The Indian Ocean Dipole (IOD) is an important ocean-atmosphere coupled phenomenon in the tropical Indian Ocean, which is characterized by a west-east dipole pattern in both sea temperature and sea level (Saji et al., 1999; Webster et al., 1999). Its positive phase shows positive sea surface temperature anomalies (SSTAs) in the western Indian Ocean and negative SSTAs in the southeastern Indian Ocean, accompanied by anomalous easterly winds at the Equator (Saji et al., 1999; Webster et al., 1999). The negative phase shows

the opposite SSTA and wind anomaly patterns. The magnitude of IOD events is asymmetric, with positive events usually larger than negative ones (Vinayachandran et al., 2002; Ashok et al., 2003). IOD events affect not only the precipitation and land surface temperature in nearby regions by modulating the monsoons (Ansell et al., 2000; Behera et al., 2005; Ding et al., 2010), but also the climate in areas farther away, such as Northeast Asia, Europe, North America, and South Africa, via the evolution of planetary waves (Guan and Yamagata, 2003; Saji and Yamagata, 2003). Although the magnitude of negative IOD events is smaller than that of positive ones, their climate effects are not negligible. For example, the strong negative IOD event in 2016 caused

* Corresponding author (email: duanws@lasg.iap.ac.cn)

extreme wet conditions in Indonesia and Australia and devastating drought in East Africa (Lim and Hendon, 2017). Furthermore, there are significantly more tropical cyclones over the Southeast Indian Ocean in September–November during negative IOD events than during positive IOD events (Li et al., 2015). Therefore, studies of the predictability of IOD events, including negative ones, are meaningful and urgently needed.

Recent studies have shown that the lead time for skillful predictions of IOD events is about three to four months, and can extend to two seasons for strong events (Wajsowicz, 2004; Luo et al., 2005, 2007; Shi et al., 2012; Li and Ding, 2013). Initial sea temperature errors have been identified as one of the main factors causing the low forecast skill of IOD events. Luo et al. (2007) showed that the Scale Interaction Experiment-Frontier Research Center for Global Change (SINTEX-F) model did not successfully forecast the cold signal in the east pole of IOD events in 1997, which was mainly due to the initial sea temperature errors in the subsurface Indian Ocean. Wajsowicz (2005) suggested that the initial sea temperature errors in the subsurface Indian Ocean constrain the forecast skill of IOD events. Feng et al. (2014) showed that initial sea temperature errors with a west-east dipole pattern in the tropical Indian Ocean are most likely to cause the forecast skill of positive IOD events to decrease rapidly across the boreal winter and induce the winter predictability barrier (WPB) phenomenon. The existence of the WPB greatly limits the forecast skill of positive IOD events (Luo et al., 2007). These studies analyzed the important role of initial sea temperature errors in IOD predictions, with a particular focus on those in the tropical Indian Ocean.

It is well known that the Pacific and Indian oceans are connected via the Walker circulation and Indonesian throughflow (Lee et al., 2002; Xie et al., 2009; Yuan et al., 2011, 2013; Lian et al., 2014; Wang et al., 2018). El Niño–Southern Oscillation (ENSO), as the dominant ocean–atmosphere coupled phenomenon in the tropical Pacific Ocean, has significant effects on the occurrence and development of IOD events through the Walker circulation, the South Asian monsoon, and ocean waves (Alexander et al., 2002; Li et al., 2003; Shi et al., 2007; Wang and Wang, 2014; Guo et al., 2015; Zhang et al., 2015; Mu and Ren, 2017). Stuecker et al. (2017) demonstrated that almost two-thirds of IOD events are accompanied by ENSO (Saji et al., 1999; Loschnigg et al., 2003). Li et al. (2003) showed that ENSO is one external forcing that induces the occurrence of IOD events. Moreover, Song et al. (2007, 2008) pointed out that the warm water volume anomalies in the western and central Pacific Ocean are a precursor signal of positive IOD events. Um-menhofer et al. (2013) suggested that the heat content anomalies in the western Pacific Ocean play a critical role in the asymmetry of the east pole of IOD events. That is, in addition to ENSO, other signals in the tropical Pacific Ocean

also greatly affect IOD events.

The Pacific Ocean affects not only the development but also the prediction of IOD events. Ding and Li (2012) found that during ENSO events, a weak spring persistent barrier exists in the SSTAs of the tropical western Indian Ocean and a strong winter persistent barrier appears in the SSTAs of southeast Indian Ocean. Luo et al. (2007) showed that the forecast skill of IOD events decreases quickly in winter, then rebounds in late winter and early spring, and finally decreases rapidly again in late spring and early summer, and that the latter predictability barrier is closely related to the Pacific Ocean. Feng and Duan (2018) revealed that, as well as the WPB, a summer predictability barrier also exists in positive IOD predictions, which is closely related to initial sea temperature errors in the tropical Pacific Ocean.

Based on above discussions, to improve the forecast skill of IOD events, the role of the tropical Pacific Ocean in IOD predictions should also be considered. Furthermore, previous studies have mainly discussed positive IOD events, and there are few and limited studies on the predictability of negative IOD events. Considering the substantial climate effects of negative IOD events and the limited studies on them, in this study we focus on the role of initial sea temperature errors in the tropical Pacific Ocean on negative IOD events. Several questions are raised: What type of initial sea temperature errors in the tropical Pacific Ocean cause large prediction uncertainties for negative IOD events? What are the physical development mechanisms of these initial errors? Are there any precursors of negative IOD events in the tropical Pacific Ocean? If so, how do these precursors develop into negative IOD events?

Feng and Duan (2017) explored the optimal initial errors related to the WPB for positive IOD events using the reanalysis data. They assumed one IOD year in the reanalysis data as the “observation” and the 20 years around the IOD year as the “predictions” to this “observation”. As there are no model errors, the prediction errors here were caused only by the initial errors. Based on these assumptions, the initial errors related to the WPB were analyzed. Similarly, the approach has also been used in Kramer and Dijkstra (2013) and Zhang et al. (2015). In this study, we will answer the questions raised above using a similar method with the reanalysis data.

2. Data and method

In consideration that, the new version of Simple Ocean Data Assimilation reanalysis dataset (SODA 3.3.1) only covers the period 1980–2015, the old version of SODA 2.2.4 (Carton and Giese, 2008) is used to obtain lots of negative IOD events and discuss the effects of the Pacific Ocean on their predictability. The sea temperature and wind stress are

derived from the data for the period 1921–2008. The horizontal resolution is $0.5^\circ \times 0.5^\circ$ and the vertical resolution varies with depth. Mann et al. (1998) demonstrated that the dominant forcing in the twentieth century is the increase in greenhouse gases; therefore, by removing the linear trend from the data, the effects of the varying forcing can be ignored. Based on this, the reanalysis dataset with linear trend removed is assumed as the output of a perfect model with a time-invariant forcing and applied in the following discussions.

To explore the initial errors that cause large prediction uncertainties for negative IOD events, ten negative IOD events (i.e., the dipole mode index (DMI), which is defined as the difference in SSTAs between the west and east poles of IOD events, is smaller than -0.5 standard deviations for three consecutive months) were randomly selected from the reanalysis data (Figure 1), and the sea temperatures of these IOD events were taken as the “observations” (i.e., the reference states) to be predicted. Then for each negative IOD event, the sea temperatures of the 10 years preceding it and the 10 years following it were taken as the “predictions” for the “observation”. That is, there are 20 “predictions” for one “observation”. Each “prediction” has a lead time of 12 months. The start months of these “predictions” are July (–1), October (–1), and January (0), respectively, where –1 indicates the year preceding the IOD year, and 0 signifies the IOD year. As the results are similar among different start months, only results for start month October (–1) are shown in this study. Specifically, the sea temperatures from October (–1) to September (0) in each reference IOD year were seen as the “observations”, and the sea temperatures from October (–2) to September (–1) (where –2 denotes the year preceding the year –1) were considered as one of the 20 “predictions”, and so on. Considering that the forcing was assumed time-invariant and that there are no model errors in “predictions”, the different “predictions” here are caused only by different initial fields. That is, the prediction errors are caused only by initial errors. The initial errors are defined as the difference in sea temperatures in October (–1) between the “predictions” and the corresponding “observation”. In view of the important role of the initial errors in the tropical Indian and Pacific oceans on IOD predictions, only the initial errors in these areas (i.e., $50^\circ\text{E}–90^\circ\text{W}$, $10^\circ\text{S}–10^\circ\text{N}$) are analyzed. Similarly, the prediction errors are defined as the absolute values of the difference in DMI between the “predictions” and the corresponding “observation”. The growth rates of prediction errors are symbolized as κ and defined as:

$$\kappa = \frac{\partial P(t)}{\partial t} \approx \frac{P(t_2) - P(t_1)}{t_2 - t_1}, \quad (1)$$

where $P(t_1)$ and $P(t_2)$ represent the prediction errors at time t_1 and t_2 ($t_2 > t_1$), respectively. When the value of κ is positive

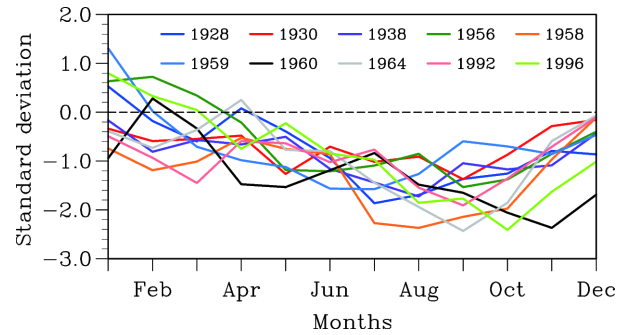


Figure 1 DMIs of 10 reference negative IOD events. 1928, 1930, ..., and 1996 indicate the years of 10 reference negative IOD events.

(negative), the prediction errors increase (decrease). The larger the positive growth rates, the faster the prediction errors grow.

To explore the precursors of negative IOD events, a similar method is applied. A major difference is that ten normal years (i.e., years that are not positive or negative IOD events) were selected from the reanalysis data and the sea temperatures of these normal years were taken as the “observations” (i.e., the reference states) to be predicted. The sea temperatures in the 10 years preceding and 10 years following each normal year were taken as the “predictions” for each “observation”. That is, there are 20 “predictions” with a lead time of 12 months for each reference normal year. As the DMIs of IOD events usually reverse sign in winter (Wajso-wicz, 2004), i.e., IOD events generally occur in winter, the start month of these “predictions” here is defined as January (0). Thus, the initial perturbations superimposed on the initial field of the reference normal year are defined as the difference in sea temperatures of the tropical Indian and Pacific oceans (i.e., $50^\circ\text{E}–90^\circ\text{W}$, $10^\circ\text{S}–10^\circ\text{N}$) in January (0) between the “predictions” and the corresponding “observation”. The development of these initial perturbations is described by the difference in sea temperatures between the “predictions” and the “observation”. If the predicted DMI is smaller than -0.5 for at least three months, a negative IOD event occurs. Then, the corresponding initial perturbation is seen as one precursor of negative IOD events.

3. Predictability barriers of negative IOD events caused by initial sea temperature errors

In this section, we first analyze the seasonal evolution of prediction errors and identify the predictability barrier phenomena in predictions of negative IOD events. Then initial errors that are most likely to cause a significant predictability barrier, as well as their physical development mechanisms, are analyzed.

3.1 Spatial patterns of initial errors that cause a significant SPB phenomenon

For the 10 reference negative IOD events, we calculated the prediction errors in each “prediction”. The prediction errors tend to grow fastest in summer (i.e., May to July) and yield SPBs in some “predictions” (Figure 2), while no SPB occurs in other “predictions” (Figure 3). That is, some initial errors are inclined to yield a SPB, while others are not. If taking the mean of the “predictions” of 10 reference IOD events, it is also found that the mean prediction error grows fastest in summer and yields a SPB (figure omitted). That is, a significant SPB exists in predictions of negative IOD events.

To further analyze the effects of initial errors on negative IOD predictions, we defined the DMI errors as the difference in DMI between the “predictions” and the corresponding “observation” (see eq. (2)). Therefore, for one reference IOD event (i.e., “observation”), the mean DMI error of the 20 “predictions” is equal to the difference in DMI between the ensemble mean of the 20 “predictions” and the corresponding “observation” (see eq. (3)). As the ensemble mean of the 20 “predictions” is similar to the climatology, the mean DMI error is closely related with this climatology and the reference IOD event. Actually, the right side of eq. (3) describes the evolution of anomalous sea temperature of IOD events (with reversed signs) and has similar dynamical behavior to that of the mean DMI error in the left side of the equation. As Figure 4 shows that the mean DMI errors for

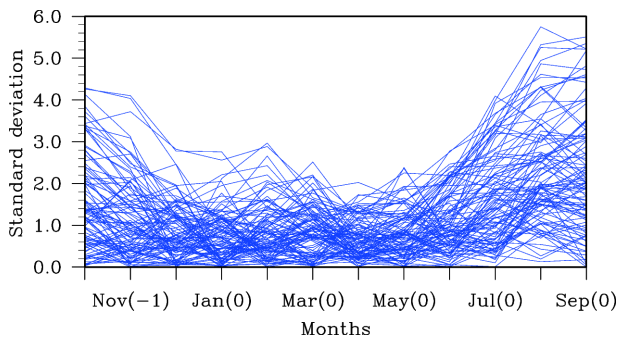


Figure 2 Time-dependent evolution of prediction errors that yield SPBs. -1 on the x-axis indicates the year preceding the IOD year, and 0 signifies the IOD year.

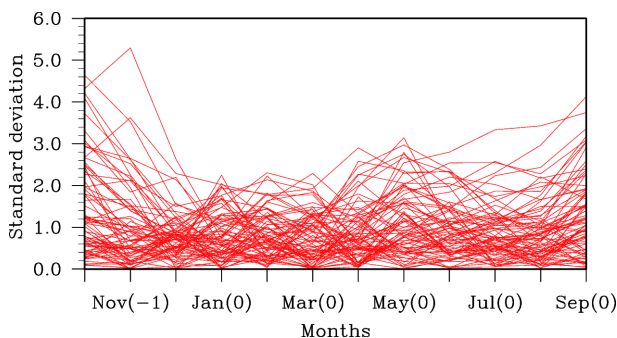


Figure 3 As in Figure 2 but for “predictions” without SPBs.

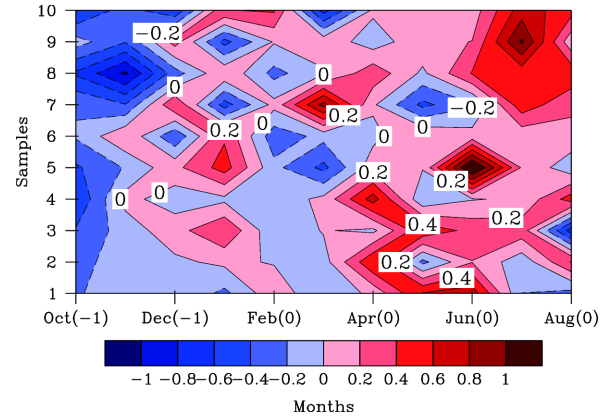


Figure 4 Ensemble mean of the monthly growth rates of prediction errors for each reference IOD event (units: month⁻¹). The horizontal axis denotes the months from October (-1) to August (0), where -1 indicates the year preceding the IOD year, and 0 signifies the IOD year. The vertical axis denotes the 10 reference IOD events.

most reference IOD events grow fastest in summer, which is consistent with the results in Figure 2 and verify the existence of SPB, this, together with eq. (3), indicates that most reference IOD events are also inclined to grow fastest in summer.

Denote the DMI error in each “prediction” as E_i , then

$$E_i = P_i - O, \quad (2)$$

where P_i and O respectively indicate the predicted and observed DMI in the i th “prediction”. By calculating the ensemble mean of the 20 “predictions”, we obtained the mean DMI error \bar{E} , which is calculated as

$$\bar{E} = \frac{1}{20} \sum_{i=0}^{20} E_i = \frac{1}{20} \sum_{i=0}^{20} P_i - O = C - O, \quad (3)$$

where C can be approximate to the climatology.

It is shown that some initial errors are inclined to yield SPBs, while others are not. Therefore, we selected initial errors that are favorable for the occurrence of a significant SPB and identified their dominant spatial patterns. In particular, initial errors that grow fastest in summer (i.e., May–July) are selected as the ones that are most likely to cause a significant SPB and defined as SPB-related initial errors. By conducting empirical orthogonal functions (EOF) analysis on these initial errors, we obtained the first mode (i.e., EOF1; responsible for 34.0% of the total variance) of SPB-related initial errors, which describes the dominant spatial patterns of initial errors that are most likely to yield a significant SPB. The corresponding time series (i.e., PC1) has positive and negative values, indicating that some initial errors are similar to the EOF1 mode, while others have the opposite spatial pattern. Therefore, according to the sign of the values in the PC1, initial errors corresponding to the positive values of PC1 are selected, and their composite is defined as type-1 initial errors (Figure 5). Similarly, the composite of initial errors corresponding to the negative values of PC1 is defined as type-2 initial errors.

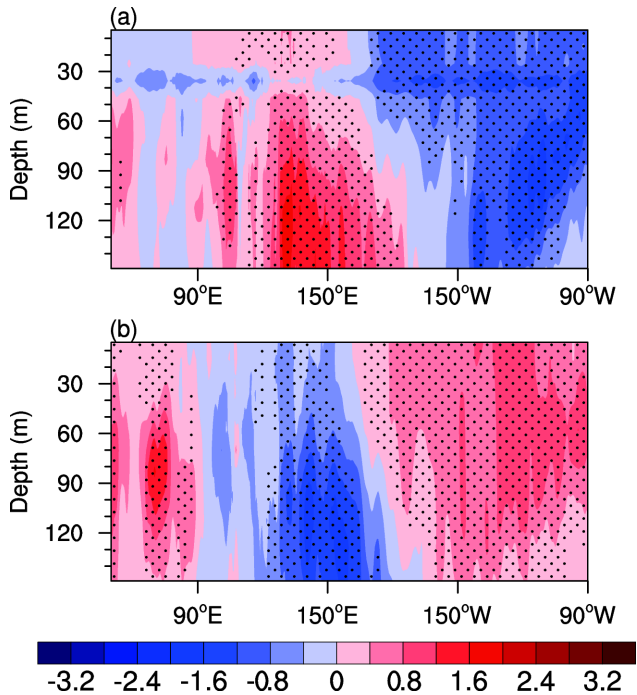


Figure 5 Spatial patterns of the equatorial (5°S–5°N) temperature profile of the (a) type-1 initial errors, (b) type-2 initial errors (units: °C). Dotted areas indicate that the composites of temperature errors exceed the 95% significance level, as determined by the *t*-test.

Type-1 initial errors show a significant west-east dipole pattern in the tropical Pacific Ocean with positive errors in the subsurface western Pacific Ocean and negative errors in the upper eastern Pacific Ocean. In contrast, the initial temperature errors in the tropical Indian Ocean are relatively small. For type-2 initial errors, the temperature errors in the tropical Pacific Ocean are almost opposite to those for type-1 initial errors. That is, negative temperature errors appear in the subsurface western Pacific Ocean, and positive errors in the upper eastern Pacific Ocean. Compared with the large temperature errors in the tropical Pacific Ocean, a weak west-east dipole pattern appears in the tropical Indian Ocean, with relatively strong positive errors in the western Indian Ocean and weak negative errors in the eastern Indian Ocean. Therefore, the initial errors are large and significant in the tropical Pacific Ocean for the two types of SPB-related initial errors, which suggests that the initial errors in the tropical Pacific Ocean probably play an important role in yielding a significant SPB. In contrast, the initial errors in the tropical Indian Ocean are relatively small, and even insignificant for type-1 initial errors. This implies that the initial errors in the tropical Indian Ocean might not be necessary for the occurrence of a significant SPB. That is, the SPB is probably closely related to the initial errors in the tropical Pacific Ocean. To further identify the roles of initial errors in the tropical oceans on IOD predictions, the development of the two types of initial errors are analyzed.

3.2 Physical development mechanisms for SPB-related initial errors

When type-1 initial errors are superimposed on the initial field of the reference-state IOD event, positive SST errors appear in the western Pacific Ocean and negative SST errors in the eastern Pacific Ocean (Figure 6). Meanwhile, a weak west-east dipole pattern of SST errors appears in the tropical Indian Ocean. It is found that the negative SST errors in the central and eastern Pacific Ocean are maintained only in the first half of the prediction year, and then reverse into positive SST errors in the second half of the prediction year. That is, the development of SST errors in the tropical Pacific Ocean is similar to the decaying phase of La Niña, and then transition to the growing phase of a weak El Niño. The strong negative SST errors in the central and eastern Pacific Ocean induce strong easterly wind anomalies at the Equator. Correspondingly, strong westerly wind anomalies appear in the tropical Indian Ocean. As the zonal gradient of the SST errors in the tropical Indian Ocean is weak, we inferred that the strong westerly wind anomalies are not mainly induced by the local SST errors. Furthermore, Chen (2010) and Lian et al. (2014) showed that the SST anomalies in the tropical Pacific Ocean can modulate the wind fields in the tropical Indian Ocean through the Walker circulation over the tropical oceans. Therefore, the strong westerly wind anomalies in the tropical Indian Ocean are probably induced by the SST errors in the tropical Pacific Ocean. In response to the anomalous westerly wind, warm water is piled up in the eastern Indian Ocean, and as a result, cold water is supplemented in the western Indian Ocean, resulting in a significant west-east dipole pattern in the subsurface ocean. Furthermore, the anomalous westerly winds have a similar wind direction to the climatological wind field (figures omitted), especially in the eastern Indian Ocean, which increases the total wind speed and thus the release of latent heat flux. This further suppresses the warming of the sea surface water in the eastern Indian Ocean, resulting in a basin-wide cooling mode of SST errors. In the second half of the prediction year, with the decaying of negative SST errors and the appearance of positive SST errors in the central and eastern Pacific Ocean, the anomalous easterlies reverse to anomalous westerlies at the Equator. Meanwhile, anomalous easterly winds appear in the tropical Indian Ocean, which are probably induced under the combined effects of the SST errors in the tropical Pacific and Indian oceans and further amplified under the Bjerknes positive feedback. The anomalous easterly winds are favorable for the piling up of warm water in the western Indian Ocean, and cooling the sea water in the eastern Indian Ocean, causing a west-east dipole pattern in the tropical Indian Ocean. In summer, the climatological wind field reverses into southeast winds, which increases the total wind speed in the southeastern Indian Ocean and thus

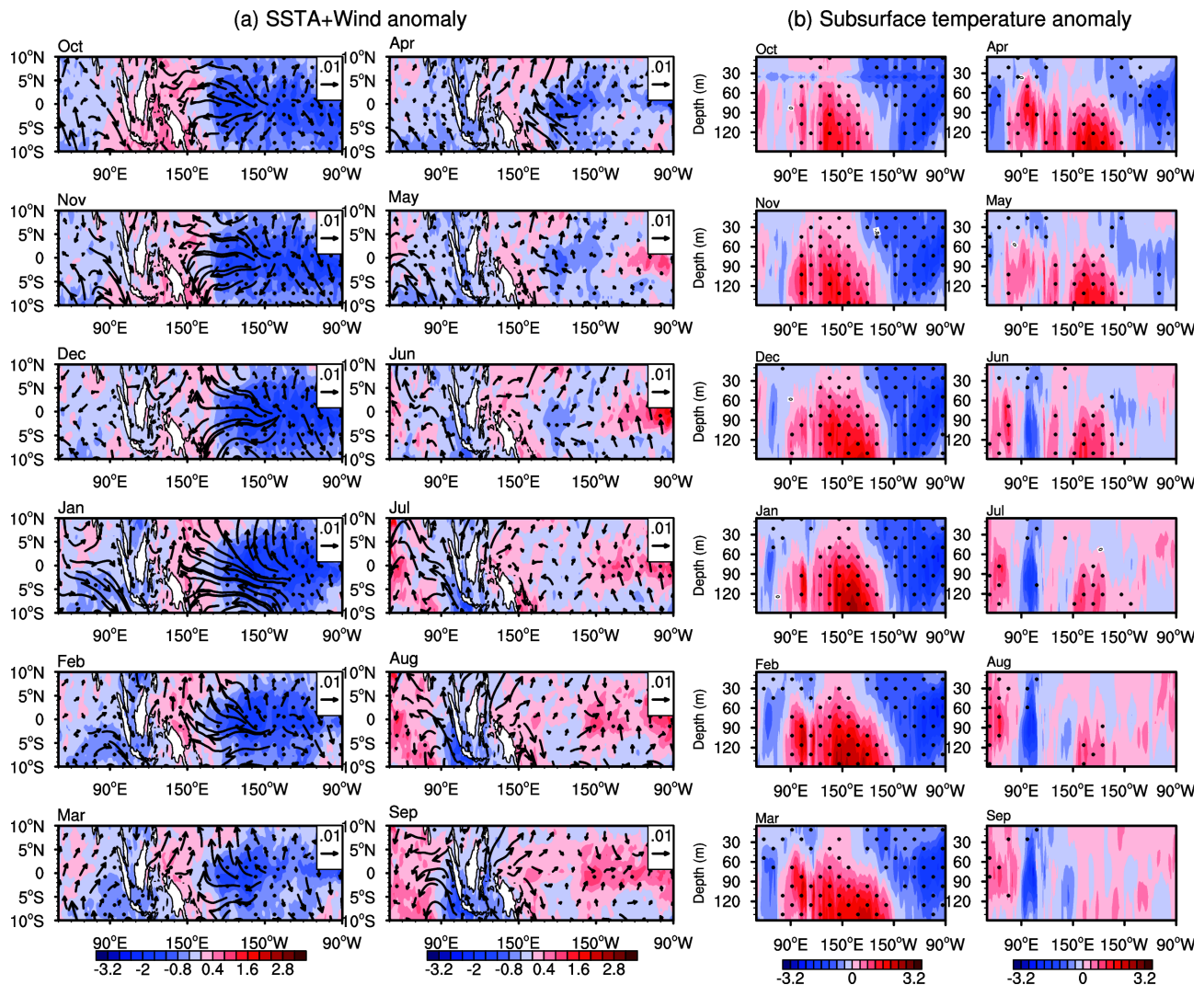


Figure 6 Evolutions of the SSTAs (units: $^{\circ}\text{C}$) and sea surface wind stress anomalies (units: N m^{-2}) over the tropical Indian and Pacific oceans (a) and the equatorial (5°S – 5°N) subsurface temperature anomalies (units: $^{\circ}\text{C}$) (b) for the type-1 initial errors. Dotted areas indicate that the composites of temperature errors exceed the 95% significance level, as determined by the t -test.

the release of latent heat flux. This further cools the sea water in the southeastern Indian Ocean and strengthens the zonal gradient of SST errors in the tropical Indian Ocean, causing a fast growth of DMI errors (i.e., prediction errors) and thus a significant SPB.

When type-2 initial errors are superimposed on the initial field of the reference-state IOD event, a significant west-east dipole pattern of SST errors appears in the tropical Pacific Ocean, with negative errors in the western Pacific Ocean and positive errors in the eastern Pacific Ocean (Figure 7). Different from the development of type-1 initial errors in the tropical Pacific Ocean, the development of SST errors in the tropical Pacific Ocean is similar to the decaying phase of an El Niño event. In response to the zonal gradient of the SST errors in the tropical Pacific Ocean, strong westerly anomalies appear at the Equator and are maintained for the whole prediction year. In the meantime, a weak west-east dipole pattern of SST errors is superimposed in the tropical

Indian Ocean, with a small area of negative errors concentrated in Sumatra and Java. Then strong easterly wind anomalies appear in the tropical Indian Ocean and are maintained for most of the prediction year, which are probably induced by the SST errors in the tropical Pacific Ocean via modulation of the Walker circulation in the tropical oceans. Under the effects of anomalous winds, warm water is piled up in the western Indian Ocean and cold water is supplemented by the upwelling in the eastern Indian Ocean, resulting in a significant west-east dipole pattern in the subsurface Indian Ocean. As the easterly wind anomalies have the opposite wind direction to the climatological winds, especially in the eastern Indian Ocean in winter and spring, which decreases the total wind speed and thus the release of latent heat flux, the sea surface water warms in the eastern Indian Ocean and forms a basin-wide warming mode of SST errors in the tropical Indian ocean. However, the climatological wind field reverses into southeast winds in summer,

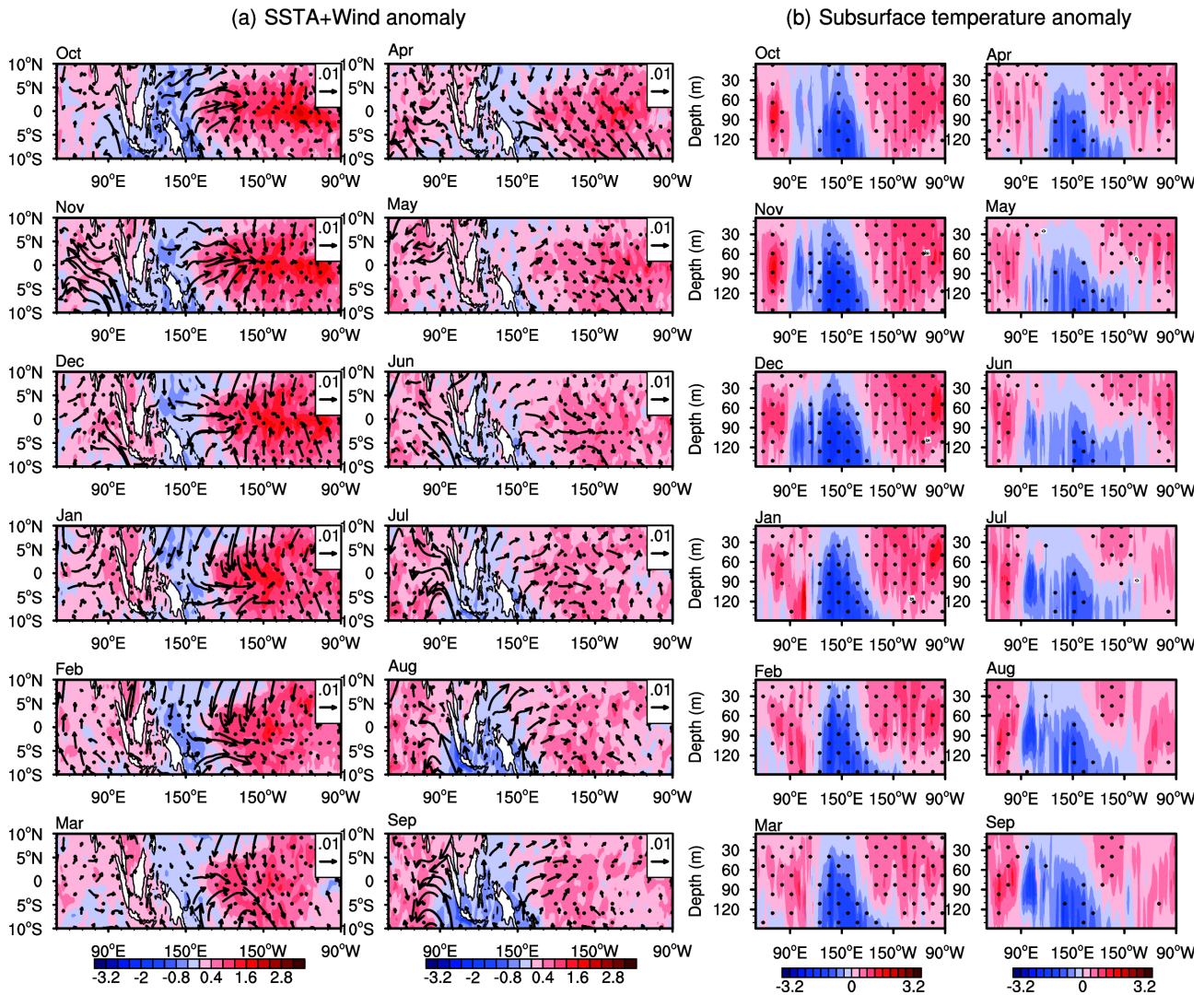


Figure 7 As in Figure 6 but for the type-2 initial errors.

which have a similar wind direction to the anomalous winds, especially in the southeastern Indian Ocean. Therefore, the total wind speed increases, adding the release of latent heat flux in the southeastern Indian Ocean, which cools the sea surface water there. This causes a significant west-east dipole pattern of SST errors in the tropical Indian Ocean, which is further strengthened under the Bjerknes positive feedback. Therefore, the DMI errors (i.e., the prediction errors) increase rapidly in summer, resulting in a significant SPB.

Based on the above discussion, two types of SPB-related initial errors cause positive SST errors in the western Indian Ocean and negative SST errors in the eastern Indian Ocean in summer. That is, the reference states are predicted as weaker negative IOD events or even as positive ones when a significant SPB phenomenon occurs. By tracking the evolution of initial errors, we found that the fast growth of prediction errors in summer is caused by the combined effects of the initial errors in the tropical Pacific Ocean and the climato-

logical wind field, which modulates the Walker circulation and further the latent heat flux errors. Therefore, the SPB phenomenon is closely related to the initial errors in the tropical Pacific Ocean. If we improve the accuracy of the initial field in the tropical Pacific Ocean by increasing the number of observations as much as possible, the SPB phenomenon may be weakened and the magnitude of negative IOD events will probably be skillfully predicted.

Feng and Duan (2018) demonstrated that a west-east dipole pattern of initial errors in the tropical Pacific Ocean is most likely to cause a significant SPB for positive IOD events, which is similar to the results for negative IOD events in this study. However, the SPB-related initial errors for positive IOD events cause negative SST errors in the western Indian Ocean and positive SST errors in the eastern Indian Ocean (i.e., negative prediction errors) in summer. Therefore, positive IOD events are generally predicted to be weaker than the “observations” when a significant SPB occurs.

4. Precursors of negative IOD events in the tropical Pacific Ocean

In this section, the dominant spatial patterns of initial perturbations that develop into negative IOD events in the tropical Indian and Pacific oceans are explored. Furthermore, the development of these precursors is also analyzed to further identify the role of initial perturbations in the tropical oceans on IOD predictions.

4.1 Dominant spatial patterns of precursors for negative IOD events

As described in Section 2, initial perturbations that develop into negative IOD events were selected as precursors of negative IOD events. Then EOF analysis was conducted to explore the dominant spatial patterns of these precursors, which is described as the first EOF mode (i.e., EOF1; responsible for 33.8% of the total variance). The corresponding time series PC1 has positive and negative values, which indicates that some precursors have similar spatial patterns to the EOF1 mode, and some have the opposite pattern. Therefore, initial perturbations corresponding to the positive values of PC1 were selected and their composite is defined as the type-1 precursor. Similarly, the composite of initial perturbations corresponding to negative values of PC1 is defined as the type-2 precursor.

The type-1 precursor presents a weak west-east dipole pattern in the tropical Indian Ocean, with positive values in the western Indian Ocean and negative values in the eastern Indian Ocean (Figure 8a). In the meantime, a significant west-east dipole pattern of initial perturbations appears in the tropical Pacific Ocean, with large negative values in the lower western Pacific Ocean and positive values in the upper eastern Pacific Ocean. Different from the type-1 precursor, negative sea temperature anomalies are shown in the tropical Indian Ocean for type-2 precursor, with the largest values located in the subsurface eastern Indian Ocean (Figure 8b). The type-2 precursor signals in the tropical Pacific Ocean are almost opposite to the type-1 precursor signals. Based on the above discussion, there are significant signals in both the tropical Indian and Pacific oceans. Do the initial perturbations in the Indian and Pacific oceans both play an important role in inducing a negative IOD event? By analyzing the evolution of these two precursors, the importance of initial perturbations in the tropical oceans will be further identified.

4.2 Physical development mechanisms for precursors of negative IOD events

When the type-1 precursor is superimposed on the initial field of the reference state (i.e., the normal years), a weak basin-wide warming of sea surface water appears in the

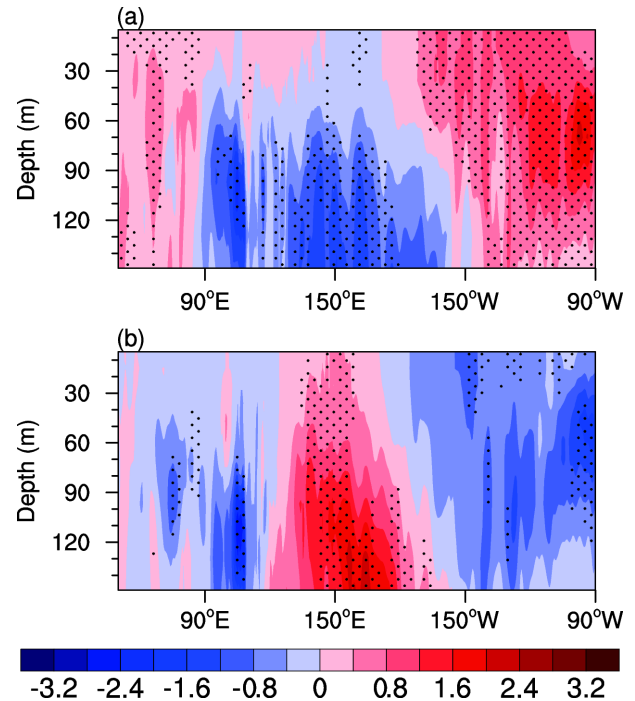


Figure 8 Spatial patterns of the equatorial (5°S–5°N) temperature profile of the (a) type-1 precursor, (b) type-2 precursor (units: °C). Dotted areas indicate that the composites of the temperature anomalies exceed the 95% significance level, as determined by the *t*-test.

tropical Indian Ocean (Figure 9). In the meantime, a west-east dipole pattern of SSTAs appears in the tropical Pacific Ocean, accompanied by a significant dipole pattern of temperature anomalies in the subsurface Pacific Ocean. The development of the SSTAs in the tropical Pacific Ocean is similar to the decaying phase of an El Niño event, which decays within the first few months. In response to the large zonal gradient of SSTAs in the tropical Pacific Ocean in January, strong westerly wind anomalies appear in the western and central Pacific Ocean, which further induce easterly wind anomalies in the tropical Indian Ocean by modulating the Walker circulation in the tropical oceans (Chen, 2010; Lian et al., 2014). In winter and early spring, the easterly wind anomalies have the opposite wind direction to the climatological northwest winds, especially in the southeastern Indian Ocean, which decreases the total wind speed and thus the release of latent heat flux, finally warming the sea surface water there. With the decaying of large positive SSTAs in the tropical Pacific Ocean, the sea surface wind anomalies in the tropical Indian Ocean are gradually controlled by the local SSTAs. Therefore, in response to the positive SSTAs in the southeastern Indian Ocean, northwest wind anomalies appear in the tropical Indian Ocean. In late spring and summer, the climatological wind reverses into southeast winds, especially in the southeastern Indian Ocean. Therefore, the northwest wind anomalies reduce the total wind speed, especially in the southeastern Indian Ocean, and thus de-

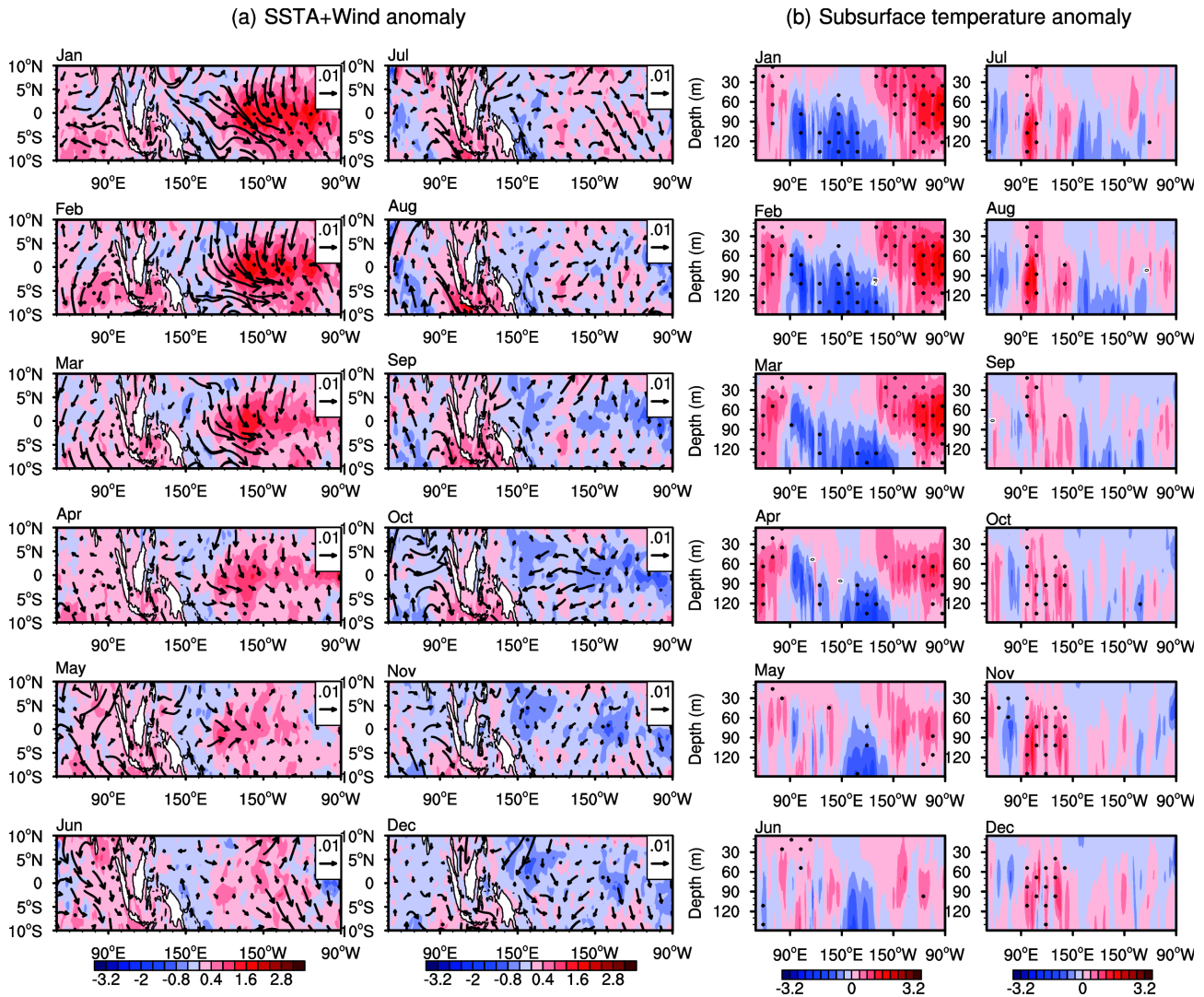


Figure 9 As in Figure 6 but for the type-1 precursor.

crease the release of the latent heat flux, finally warming the sea surface water there. Furthermore, the northwest wind anomalies also pile up warm water in the southeastern Indian Ocean, and cold water is supplemented in the western Indian Ocean, which amplifies the zonal gradient of SSTAs in the tropical Indian Ocean and in turn strengthens the northwest wind anomalies. Therefore, a significant west-east dipole pattern of SSTAs appears under the Bjerknes positive feedback, and a negative IOD event occurs.

When the type-2 precursor is superimposed on the initial field of the reference state (i.e., the normal years), a weak northwest-southeast dipole pattern of SSTAs appears in the tropical Indian Ocean, with a small area of positive SSTAs concentrated in the southeastern Indian Ocean (Figure 10). Meanwhile, a significant west-east dipole pattern of SSTAs is shown in the tropical Pacific Ocean, with weak positive SSTAs in the western Pacific Ocean and strong negative SSTAs in the central and eastern Pacific Ocean. The devel-

opment of the SSTAs in the tropical Pacific Ocean is similar to the decaying phase of a La Niña event, and the SSTAs decay rapidly within the first few months. In January, the weak northwest-southeast dipole pattern of SSTAs favors the appearance of northwest wind anomalies in the tropical Indian Ocean. Furthermore, the strong zonal gradient of SSTAs in the tropical Pacific Ocean induces strong easterly wind anomalies, which further induces westerly wind anomalies in the tropical Indian Ocean by modulating the Walker circulation in the tropical oceans (Chen, 2010; Lian et al., 2014) and strengthens the northwest wind anomalies there. That is, the northwest wind anomalies are probably induced and maintained under the combined effects of local and remote SSTAs in the first few months. In late spring and summer, with the reversal of climatological winds, the northwest wind anomalies are favorable for the warming of sea surface water in the southeastern Indian Ocean and thus the appearance of a west-east dipole pattern, which is similar to the develop-

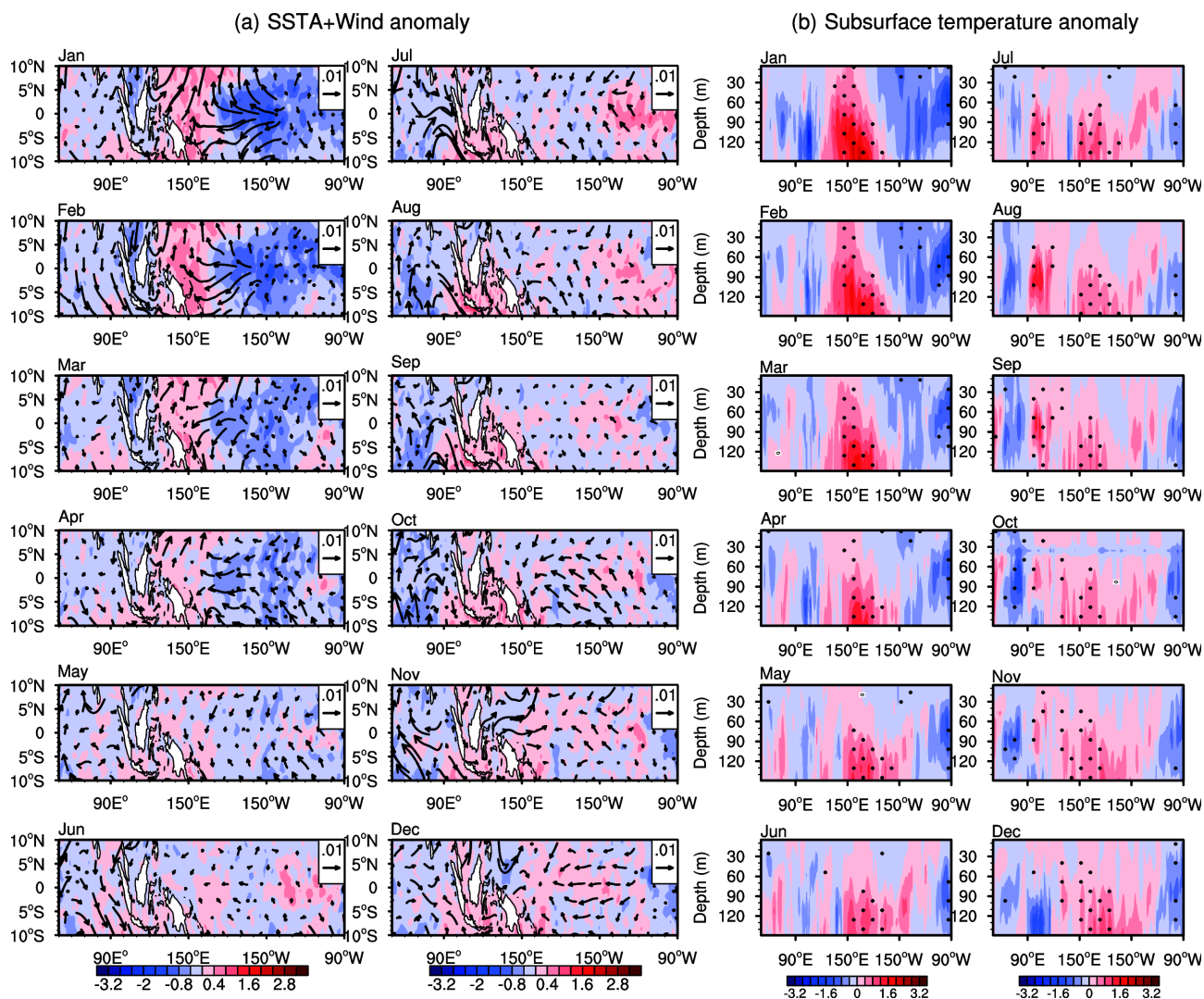


Figure 10 As in Figure 6 but for the type-2 precursor.

ment of the type-1 precursor. Finally, a negative IOD event occurs.

Based on the above discussion, although the spatial patterns of the two types of precursors are different, under the combined effects of SSTAs in the tropical Indian and Pacific oceans, they both develop and induce northwest wind anomalies in the tropical Indian Ocean, which favor the occurrence of a negative IOD event. Furthermore, as discussed in Section 3, the initial errors in the tropical Pacific Ocean with a west-east dipole pattern are more inclined to cause a significant SPB and induce large prediction uncertainties for IOD events. Therefore, intensive observations over the tropical Pacific Ocean will not only improve the accuracy of the initial field and reduce the prediction errors in summer, but also detect the precursor signals of negative IOD events in advance, which will greatly improve the forecast skill for negative IOD events.

5. Summary and discussion

In this study, we explored the effects of initial sea temperature errors in the tropical Indian and Pacific oceans on the predictability of negative IOD events using reanalysis data. Furthermore, precursors of negative IOD events in the tropical Indian and Pacific oceans were also analyzed.

A significant SPB phenomenon exists in predictions of negative IOD events, when considering initial errors in the tropical Indian and Pacific oceans. There are two types of initial errors that are most likely to induce a significant SPB. Type-1 initial errors show a significant west-east dipole pattern in the tropical Pacific Ocean, accompanied by relatively small initial errors in the tropical Indian Ocean. Type-2 initial errors have an opposite spatial pattern in the tropical Pacific Ocean to type-1 initial errors, accompanied by a weak west-east dipole pattern in the tropical Indian Ocean. Therefore, SPB-related initial errors in the tropical Pacific

Ocean are large and significant. In contrast, initial errors in the tropical Indian Ocean are relatively small. This suggests that the SPB is probably closely related to initial errors in the tropical Pacific Ocean and that the role of initial errors in the tropical Indian Ocean is negligible.

The development of the type-1 initial errors in the tropical Pacific Ocean is similar to the decaying phase of a La Niña event, and then transitions into the growing phase of a weak El Niño event. In the first half of the prediction year, strong easterly wind anomalies are induced by the SST errors in the tropical Pacific Ocean, which further induce strong westerly wind anomalies in the tropical Indian Ocean by modulating the Walker circulation in the tropical oceans. The anomalous westerly wind piles up warm water in the eastern Indian Ocean, and thus cold water is supplemented in the western Indian Ocean. Furthermore, it also increases the total wind speed, especially in the southeastern Indian Ocean, and thus the release of the latent heat flux, which cools the sea surface water there and causes a basin-wide cooling mode of SST errors in the tropical Indian Ocean. In the second half of the prediction year, the anomalous westerlies reverse to anomalous easterlies in the tropical Indian Ocean, which piles up warm water in the western Indian Ocean and thus cold water is supplemented in the eastern Indian Ocean. Meanwhile, the climatological winds reverse into southeast winds in the southeastern Indian Ocean. Therefore, the anomalous easterlies increase the total wind speed and cool the sea surface water in the southeastern Indian Ocean by releasing more latent heat flux, which strengthens the zonal gradient of SST errors and causes a fast growth of prediction errors under the Bjerknes positive feedback, resulting in a significant SPB.

Different from the type-1 initial errors, the development of the type-2 initial errors in the tropical Pacific Ocean is similar to the decaying phase of an El Niño event. Therefore, strong westerly wind anomalies appear in the tropical Pacific Ocean and are maintained for most of the prediction year, which further induce easterly wind anomalies in the tropical Indian Ocean by modulating the Walker circulation in the tropical oceans. In the first half of the prediction year, the anomalous easterly wind piles up warm water in the western Indian Ocean, and thus cold water is supplemented in the eastern Indian Ocean. Furthermore, the anomalous winds have the opposite wind direction to the climatological winds, especially in the southeastern Indian Ocean, which warms the sea surface water there by decreasing the release of the latent heat flux and forms a basin-wide warming mode in the tropical Indian Ocean. In the second half of the prediction year, the development of SST errors is similar to that for type-1 initial errors, finally yielding a significant SPB. It is found that the SPB is mainly caused by the combined effects of initial errors in the tropical Pacific Ocean and the climatological wind field.

In addition to the SPB-related initial errors, the precursors

of negative IOD events were also analyzed. Similarly, there are two types of precursors. The type-1 precursor shows a weak west-east dipole pattern in the tropical Indian Ocean and a significant dipole pattern in the tropical Pacific Ocean. The type-2 precursor has the opposite spatial pattern to the type-1 precursor in the tropical Pacific Ocean, accompanied by negative temperature anomalies in the tropical Indian Ocean. Unlike negative events, Song et al. (2007, 2008) emphasized that the precursor of positive IOD events were concentrated in the western and central Pacific Ocean.

Although the two types of precursors have different spatial patterns, under the combined effects of local (i.e., tropical Indian Ocean) and remote (i.e., tropical Pacific Ocean) temperature anomalies, northwest wind anomalies appear in the tropical Indian Ocean in the first few months. With the decaying of SSTAs in the tropical Pacific Ocean, the northwest wind anomalies are mainly controlled by the local SSTAs in the rest of the prediction year. On the one side, the northwest wind anomalies pile up warm water in the southeastern Indian Ocean, and as a result cold water is supplemented in the western Indian Ocean. On the other side, the climatological wind reverses direction into southeast winds in late spring and summer, especially in the southeastern Indian Ocean. The northwest wind anomalies reduce the total wind speed and thus the loss of the latent heat flux, warming the sea surface water in the southeast Indian Ocean. This induces a west-east dipole pattern of SSTAs, which is further strengthened under the Bjerknes feedback, yielding a negative IOD event. Therefore, in addition to the precursor signals in the tropical Indian Ocean, the temperature anomalies in the tropical Pacific Ocean also play an important role in inducing a negative IOD event.

Based on above discussion, the Pacific Ocean plays an important role in predictions of negative IOD events. Intensive observations in the tropical Pacific Ocean would not only improve the accuracy of the initial field and weaken the SPB phenomenon, but also detect the precursor signals of negative IOD events in advance, which would largely improve the forecast skill of negative IOD events. Furthermore, previous studies have demonstrated that initial errors in the tropical Indian Ocean can cause a WPB phenomenon, which greatly limits the forecast skill of IOD events. Then, which ocean plays a more important role in IOD predictions, the tropical Indian Ocean or the tropical Pacific Ocean? To further answer this question, sensitivity experiments should be conducted to identify the relative role of the tropical oceans in IOD predictions. Furthermore, as well as the initial temperature errors and initial temperature anomalies in the tropical Indian and Pacific oceans, other atmospheric and oceanic variables in other oceans may also have an effect on negative IOD events and should be considered in future studies.

Acknowledgements This work was supported by the National Natural Science Foundation of China (Grant Nos. 41506032 & 41530961), and the National Programme on Global Change and Air-Sea Interaction (Grant No. GASI-IPOVAI-06).

References

- Alexander M A, Bladé I, Newman M, Lanzante J R, Lau N C, Scott J D. 2002. The atmospheric bridge: The influence of ENSO teleconnections on air-sea interaction over the global oceans. *J Clim*, 15: 2205–2231
- Ansell T, Reason C J C, Meyers G. 2000. Variability in the tropical southeast Indian Ocean and links with southeast Australian winter rainfall. *Geophys Res Lett*, 27: 3977–3980
- Ashok K, Guan Z, Yamagata T. 2003. Influence of the Indian Ocean Dipole on the Australian winter rainfall. *Geophys Res Lett*, 30: 1821
- Behera S K, Luo J J, Masson S, Delecluse P, Gualdi S, Navarra A, Yamagata T. 2005. Paramount impact of the Indian Ocean Dipole on the East African short rains: A CGCM study. *J Clim*, 18: 4514–4530
- Carton J A, Giese B S. 2008. A reanalysis of ocean climate using Simple Ocean Data Assimilation (SODA). *Mon Weather Rev*, 136: 2999–3017
- Chen D. 2010. Indo-Pacific tripole: An intrinsic mode of tropical climate variability. *Adv Geosci*, 24: 1–18
- Ding R, Ha K J, Li J P. 2010. Interdecadal shift in the relationship between the East Asian summer monsoon and the tropical Indian Ocean. *Clim Dyn*, 34: 1059–1071
- Ding R, Li J. 2012. Influences of ENSO teleconnection on the persistence of sea surface temperature in the Tropical Indian Ocean. *J Clim*, 25: 8177–8195
- Feng R, Duan W S, Mu M. 2014. The “winter predictability barrier” for IOD events and its error growth dynamics: Results from a fully coupled GCM. *J Geophys Res-Oceans*, 119: 8688–8708
- Feng R, Duan W S. 2017. IOD-related optimal initial errors and optimal precursors for IOD predictions from reanalysis data. *Sci China Earth Sci*, 60: 156–172
- Feng R, Duan W S. 2018. Investigating the initial errors that cause predictability barriers for Indian Ocean Dipole events using CMIP5 model outputs. *Adv Atmos Sci*, 35: 1305–1320
- Guan Z Y, Yamagata T. 2003. The unusual summer of 1994 in East Asia: IOD teleconnections. *Geophys Res Lett*, 30: 1544
- Guo F, Liu Q, Sun S, Yang J. 2015. Three types of Indian Ocean Dipoles. *J Clim*, 28: 3073–3092
- Kramer W, Dijkstra H A. 2013. Optimal localized observations for advancing beyond the ENSO predictability barrier. *Nonlin Processes Geophys*, 20: 221–230
- Lee T, Fukumori I, Menemenlis D, Xing Z F, Fu L L. 2002. Effects of the Indonesian throughflow on the Pacific and Indian Oceans. *J Phys Oceanogr*, 32: 1404–1429
- Li J P, Ding R Q. 2013. Temporal-spatial distribution of the predictability limit of monthly sea surface temperature in the global oceans. *Int J Climatol*, 33: 1936–1947
- Li T, Wang B, Chang C P, Zhang Y. 2003. A theory for the Indian Ocean Dipole-zonal mode. *J Atmos Sci*, 60: 2119–2135
- Li Z, Yu W, Li K, Liu B, Wang G. 2015. Modulation of interannual variability of tropical cyclone activity over Southeast Indian Ocean by negative IOD phase. *Dyn Atmos Oceans*, 72: 62–69
- Lian T, Chen D K, Tang Y M, Jin B G. 2014. A theoretical investigation of the tropical Indo-Pacific tripole mode. *Sci China Earth Sci*, 57: 174–188
- Lim E P, Hendon H H. 2017. Causes and predictability of the negative Indian Ocean Dipole and its impact on La Niña during 2016. *Sci Rep*, 7: 12619
- Loschnigg J, Meehl G A, Webster P J, Arblaster J M, Compo G P. 2003. The Asian monsoon, the tropospheric biennial oscillation, and the Indian Ocean zonal mode in the NCAR CSM. *J Clim*, 16: 1617–1642
- Luo J J, Masson S, Behera S, Shingu S, Yamagata T. 2005. Seasonal climate predictability in a coupled OAGCM using a different approach for ensemble forecasts. *J Clim*, 18: 4474–4497
- Luo J J, Masson S, Behera S, Yamagata T. 2007. Experimental forecasts of the Indian Ocean Dipole using a coupled OAGCM. *J Clim*, 20: 2178–2190
- Mann M E, Bradley R S, Hughes M K. 1998. Erratum: Global-scale temperature patterns and climate forcing over the past six centuries. *Nature*, 392: 779–787
- Mu M, Ren H L. 2017. Enlightenment from researches and predictions of 2014–2016 super El Niño event. *Sci China Earth Sci*, 60: 1569–1571
- Saji N H, Goswami B N, Vinayachandran P N, Yamagata T. 1999. A dipole mode in the tropical Indian Ocean. *Nature*, 401: 360–363
- Saji N H, Yamagata T. 2003. Structure of SST and surface wind variability during Indian Ocean Dipole mode events: COADS observations. *J Clim*, 16: 2735–2751
- Shi G, Ribbe J, Cai W, Cowan T. 2007. Multidecadal variability in the transmission of ENSO signals to the Indian Ocean. *Geophys Res Lett*, 34: L09706
- Shi L, Hendon H H, Alves O, Luo J J, Balmaseda M, Anderson D. 2012. How predictable is the Indian Ocean Dipole? *Mon Weather Rev*, 140: 3867–3884
- Song Q, Vecchi G A, Rosati A J. 2007. Indian Ocean variability in the GFDL coupled climate model. *J Clim*, 20: 2895–2916
- Song Q, Vecchi G A, Rosati A J. 2008. Predictability of the Indian Ocean sea surface temperature anomalies in the GFDL coupled model. *Geophys Res Lett*, 35: L02701
- Stuecker M F, Timmermann A, Jin F F, Chikamoto Y, Zhang W, Wittenberg A T, Widiastih E, Zhao S. 2017. Revisiting ENSO/Indian Ocean Dipole phase relationships. *Geophys Res Lett*, 44: 2481–2492
- Ummerhofer C C, Schwarzkopf F U, Meyers G, Behrens E, Biastoch A, Böning C W. 2013. Pacific Ocean contribution to the asymmetry in eastern Indian Ocean variability. *J Clim*, 26: 1152–1171
- Vinayachandran P N, Iizuka S, Yamagata T. 2002. Indian Ocean Dipole mode events in an ocean general circulation model. *Deep-Sea Res Part II-Top Stud Oceanogr*, 49: 1573–1596
- Wajswowicz R C. 2004. Climate variability over the tropical Indian Ocean sector in the NSIPP seasonal forecast system. *J Clim*, 17: 4783–4804
- Wajswowicz R C. 2005. Potential predictability of tropical Indian Ocean SST anomalies. *Geophys Res Lett*, 32: L24702
- Wang X, Wang C. 2014. Different impacts of various El Niño events on the Indian Ocean Dipole. *Clim Dyn*, 42: 991–1005
- Wang X, Tan W, Wang C. 2018. A new index for identifying different types of El Niño modoki events. *Clim Dyn*, 50: 2753–2765
- Webster P J, Moore A M, Loschnigg J P, Leben R R. 1999. Coupled ocean-atmosphere dynamics in the Indian Ocean during 1997–98. *Nature*, 401: 356–360
- Xie S P, Hu K, Hafner J, Tokinaga H, Du Y, Huang G, Sampe T. 2009. Indian Ocean capacitor effect on Indo-Western Pacific climate during the summer following El Niño. *J Clim*, 22: 730–747
- Yuan D L, Wang J, Xu T, Xu P, Hui Z, Zhao X, Luan Y, Zheng W, Yu Y. 2011. Forcing of the Indian Ocean Dipole on the interannual variations of the tropical Pacific Ocean: Roles of the Indonesian throughflow. *J Clim*, 24: 3593–3608
- Yuan D L, Zhou H, Zhao X. 2013. Interannual climate variability over the tropical Pacific Ocean induced by the Indian Ocean Dipole through the Indonesian throughflow. *J Clim*, 26: 2845–2861
- Zhang J, Duan W S, Zhi X F. 2015. Using CMIP5 model outputs to investigate the initial errors that cause the “spring predictability barrier” for El Niño events. *Sci China Earth Sci*, 58: 685–696
- Zhang W, Wang Y, Jin F F, Stuecker M F, Turner A G. 2015. Impact of different El Niño types on the El Niño/IOD relationship. *Geophys Res Lett*, 42: 8570–8576

(Responsible editor: Zhiyan ZUO)